ACADEMIC PRESS

Available online at www.sciencedirect.com

SCIENCE DIRECT®

Journal of Sound and Vibration 265 (2003) 725–743

JOURNAL OF SOUND AND VIBRATION

www.elsevier.com/locate/jsvi

Fan interaction noise reduction using a wake generator: experiments and computational aeroacoustics

C. Polacsek[a,*], F. Desbois-Lavergne[b]

[a] *Numerical Simulations and Aeroacoustics Department, ONERA, BP 72, 92322 Châtillon Cedex, France*
[b] *Applied Aerodynamics Department, ONERA, BP 72, 92322 Châtillon Cedex, France*

Received 25 April 2002; accepted 7 August 2002

Abstract

A control grid (wake generator) aimed at reducing rotor–stator interaction modes in fan engines when mounted upstream of the rotor has been studied here. This device complements other active noise control systems currently proposed. The compressor model of the instrumented ONERA CERF-rig is used to simulate suitable conditions. The design of the grid is drafted out using semi-empirical models for wake and potential flow, and experimentally achieved. Cylindrical rods are able to generate a spinning mode of the same order and similar level as the interaction mode. Mounting the rods on a rotating ring allows for adjusting the phase of the control mode so that an 8 dB sound pressure level (SPL) reduction at the blade passing frequency is achieved when the two modes are out of phase. Experimental results are assessed by a numerical approach using computational fluid dynamics (CFD). A Reynolds averaged Navier–Stokes 2-D solver, developed at ONERA, is used to provide the unsteady force components on blades and vanes required for acoustics. The loading noise source term of the Ffowcs Williams and Hawkings equation is used to model the interaction noise between the sources, and an original coupling to a boundary element method (BEM) code is realized to take account of the inlet geometry effects on acoustic in-duct propagation. Calculations using the classical analytical the Green function of an infinite annular duct are also addressed. Simple formulations written in the frequency domain and expanded into modes are addressed and used to compute an in-duct interaction mode and to compare with the noise reduction obtained during the tests. A fairly good agreement between predicted and measured SPL is found when the inlet geometry effects are part of the solution (by coupling with the BEM). Furthermore, computed aerodynamic penalties due to the rods are found to be negligible. These results partly validate the computation chain and highlight the potential of the wake generator system proposed.

*Corresponding author.
E-mail address: cyril.polacsek@onera.fr (C. Polacsek).

0022-460X/03/$ - see front matter
doi:10.1016/S0022-460X(02)01528-6

1. Introduction

Noise caused by fans during take-off and approach has become a major annoyance in high bypass ratio turbofan engines. Therefore, aircraft and engine manufacturers are facing increasing pressure to reduce exterior noise levels. For this purpose, a European Brite-Euram project called RESOUND (Reduction of Engine Source Noise through Understanding and Novel Design) started in 1998. A task of this project was devoted to laboratory experiments relative to passive/active design, one of which is at the origin of the present paper [1].

Discrete-frequency tones generated by unsteady blade row interactions are of particular concern in the design of advanced turbine engines. For subsonic fans, the acoustic tones are usually 10–15 dB above the broadband level and are mainly due to wake interaction between rotor and stator. The spatial structure of the acoustic field in the duct can be modelled using the an infinite annular duct modal expansion [2]. The acoustic field is split into propagating spinning modes described by Bessel functions. Current solutions adopted by manufacturers to quiet the fan at the source consist of selecting blade and vane number combinations to ensure that the interaction modes at the blade passing frequency (BPF) are cut off. Other basic parameters like the axial spacing between adjacent blade rows are also adjusted to try to decrease both the number and the intensity of the propagating interaction modes. Unfortunately, these methods, generally referenced as passive techniques (the same as for acoustic liner design), are becoming less efficient due to the increasing bypass ratios of turbofan engines which mean larger diameters. This is the reason why new methodologies for attenuating these modes are extensively studied today.

The most up-to-date approach is active noise control (ANC), which has been studied by many authors [3–9]. Applying the well-known anti-noise concept to fan noise reduction consists of trying to cancel the interaction modes by generating the identical out-of-phase spinning modes. The added modes are created using secondary sources. Usual ANC studies are generally based on two possibilities: (1) use of flush-mounted loudspeakers as active sources; (2) the active source is an airfoil equipped with actuators (active airfoil). The noise reduction obtained when using a sophisticated experimental set-up shows the capability of these ANC techniques. Unfortunately, applications to turbofans are not straightforward because of weight, aerodynamic penalties, and complexity of such devices. A review of the applicability of active techniques is presented in Ref. [10]. The necessity to use flow control devices is emphasized, and some suggestions are addressed. In this way, a recent study [11] also suggests a "clocking" concept that could be applied to multi-stage configurations.

Although the authors do not pretend to have exhaustive backgrounds in ANC, they propose an original contribution to such investigations, by combining both passive and active ideas, and by using an easily implemented device that could offer some industrial applications. The anti-noise system tested is a wake generator consisting of a grid of cylindrical rods. Basic investigation presented here are limited to the cancellation of a single spinning mode at the BPF. This is made by using the ONERA CERF axial compressor, and by adding an upstream grid in order to counter-balance the load fluctuations generated by interactions between the rotor and stator. The control grid is designed to generate the same propagating mode as the isolated interaction mode. The main difficulty of the concept is to adjust the amplitude and phase of this generated mode to counter-balance the interaction mode. The main parameters controlling the amplitude are the rod diameter, the rod length and the distance between the grid and the rotor.

They are roughly designed using semi-empirical models and previous CERF-rig tests, and then experimentally adjusted. The phase adjustment is made possible by mounting the rods on a rotating ring.

The first part of the paper briefly describes the CERF facility and the design of the control grid. Then, the paper focuses on the achievement of an optimal set-up with respect to acoustic noise reduction. Mode spectrum analysis and tone noise levels measured with and without the control grid system are discussed.

In a second step, experimental results are assessed by a numerical approach. For this purpose, computational fluid dynamics (CFD) and acoustic models available at ONERA have been identified, and a suitable computational chain has been investigated [12]. This numerical activity has been performed in the framework of a following Brite-Euram European project, "TurboNoiseCFD". A 3-D Reynolds averaged Navier–Stokes (RANS) code, CANARI [13], was developed at ONERA for turbomachinery computations of steady or unsteady aerodynamics. A simplified 2-D version, COLIBRI [14], is currently used for full unsteady rotor–stator configurations, which allows considerable reduction of the CPU time. RANS computations are expected to provide the unsteady blade (and vane) loads, required for acoustics. The loading noise term of the Ffowcs Williams and Hawkings (FW–H) equation [15] expresses the interaction noise due to the unsteady loads caused by potential flow or (and) wake interactions. Starting from Goldstein infinite duct theory [16], the analytical Green function is replaced by the Green function of the CERF-rig duct, numerically computed by using a commercial boundary element method (BEM) code (SysNoise), already used in Refs. [17,18]. Because the in-duct mean flow is very low (Mach number lower than 0.2), it can be assumed that the fluid is at rest, as done in the BEM code.

The paper describes the CFD solver and focuses on the acoustic computations. The computational chain is applied to the CERF-rig optimal configuration (with and without using the control grid). Aerodynamics computed by COLIBRI is compared to available measurements, in terms of blade and vane steady forces. Furthermore, steady forces are analyzed to estimate the aerodynamic penalties due to the grid. Then, unsteady forces are given to the acoustics to compute the single cut-on interaction mode, for both rotor–stator and rods–rotor configurations. The infinite duct solution is compared with the true inlet geometry solution, obtained by coupling with the BEM. Finally, interaction mode intensity and noise reduction predicted by the computations are compared to the experiment. Therefore, one can discuss the reliability of the system.

2. ONERA CERF-rig

The compressor model is 50 cm in diameter ($R = 25$ cm). The rotor has $B = 29$ blades and the downstream stator has $V = 33$ vanes. The maximum rotation speed is $N = 3500$ r.p.m., providing a mean-flow Mach number, M, close to 0.2. The centre-body is a straight cylinder with a 33.4 cm diameter, so that the duct is annular with a hub-to-tip ratio, h, equal to 0.67. The rotor/stator interaction modes are deduced from the well-known formula [2]

$$m = nB \pm jV, \tag{1}$$

Table 1
Cut-off frequency in the CERF-rig annular duct for selected azimuthal orders, m, and first radial order, $\mu = 1$

Spinning mode m	Cut-off frequency (Hz)
1	308
2	593
3	849
4	1086
5	1308
6	1537
7	1758

where n is the BPF harmonic order and j the loading harmonic order. Solving the Helmholtz equation in an infinite annular duct, the cut-off frequency of each angular and radial mode (m, μ) is given by the eigenvalues of an equation of Bessel functions of the first and second kinds, and of order m. Cut-off frequencies are given in Table 1, for some values of m, and the first radial mode, $\mu = 1$.

When the rotation speed is lower than 3500 r.p.m., the BPF ($f = BN$) is lower than 1690 Hz, which ensures modes $|m| > 6$ to be cut off on this tone. Thus, the only propagating interaction mode at the BPF is the $m = -4$ azimuthal wave number associated to the first radial mode ($\mu = 1$). These conditions are very well suited for the design of the control grid and for the numerical predictions presented in the next sections.

3. Control grid design and experimental set-up

Previous ONERA basic studies had already been devoted to noise control using control grids [19]. In these studies the acoustic sources were assumed to be on the rotor blades and to be due to the interaction between the blades and the potential velocity defect caused by the stator. Indeed, the authors of Ref. [19] investigated the possibility of directly cancelling the axial velocity defect of the flow in the rotor plane. To do that, several grids of rods were tested in the CERF-rig, in order to generate an upstream wake cancelling the potential velocity defect caused by the downstream stator.

This idea has been partly re-used in the present investigation, but in an easier way than directly trying to cancel the velocity defect (which is probably a much too complex challenge today). Here, the control grid is used to generate a wake from which a selected spatial structure of the acoustic field, i.e., a suitable spinning mode, can be obtained. For a well-designed grid, this mode should balance the rotor/stator interaction mode ($m = -4$) when both are out of phase. This concept is illustrated in Fig. 1, showing the variation of the amplitude of the interaction mode versus a reference rod azimuth, ψ. Assuming that the control mode and rotor–stator mode have exactly the same amplitude, I, the interaction mode amplitude should theoretically be get twice as much ($2I$, when modes are in phase) and vanish for an optimal azimuthal position (0, when modes are out of phase). One should note also the $2\pi/V$ azimuthal symmetry of the system.

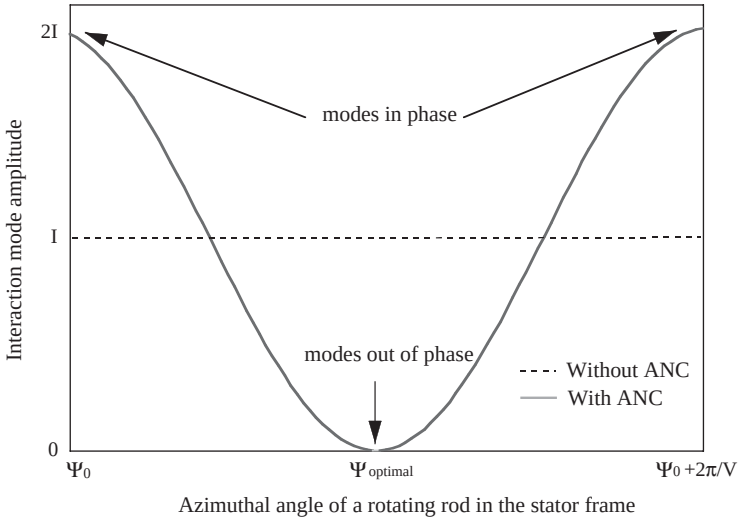

Fig. 1. Noise control system concept.

According to CERF-rig acoustic propagating conditions, a basic design should consist in choosing a grid of V' rods with $V' = V = 33$. Applying (1), this theoretically allows a grid/rotor interaction mode $m = -4$ to be created. A more clever solution is to choose V' as a submultiple of V. A smaller value for V' should be more convenient for applications. Thus, taking $V' = 11$ and $j = 3$, Eq. (1) also leads to the same mode $m = -4$, generated by the third harmonic of the rotor blade unsteady loads. The rods are chosen to be cylindrical, in order to simplify the manufacture and to lower the cost. Moreover, this helps to model the wake.

A rough design of the rods was achieved by using semi-empirical models from 2-D theories and from experiments [20–23]. A 2-D turbulent wake behind a rod and an airfoil is described by a Gaussian distribution for the mean velocity defect. Amplitude and width of the velocity defect are related to the upstream mean flow, the drag coefficient, and rod diameter (or airfoil chord). More details are given in Ref. [1]. As directed by raw design results, a grid of 11 cylindrical rods of 3 mm in diameter was mounted on a rotating ring. As a first step, the length of the rods, L, was chosen equal to the annular duct height, H ($L = H = 83$ mm). The rod to blade axis–line distance was set to 35 mm. A diagram of the experimental set-up is given in Fig. 2a. The modal analysis measurement is made using twelve $\frac{1}{4}$in microphones for each of the upstream and downstream rings. This number is well suited to the modal bandwidth at the BPF ($|m| < 6$), as is shown in the first section. The rotor–stator axial distance was adjusted to its minimum value to ensure that the interaction mode $m = -4$ was highly dominant with respect to the background noise level. In the same way, non-rotor noise is largely reduced due to a synchronous modal analysis triggered on a one-per-rev pulse.

The rotating rods system is sketched in Fig. 2b. The rods are mounted on a rotating ring attached to the casing and manually displaced in the azimuthal direction. Concerning the adjustment of the phase, the azimuth range for positioning of the rods can be limited to $2\pi/33$, because of the $2\pi/V$ symmetry mentioned above. Since the azimuth position is not automatically achieved here (which would require a feedback controller), the noise control proposed is purely passive. However, by extension, one sometimes speaks of ANC-like system in the paper.

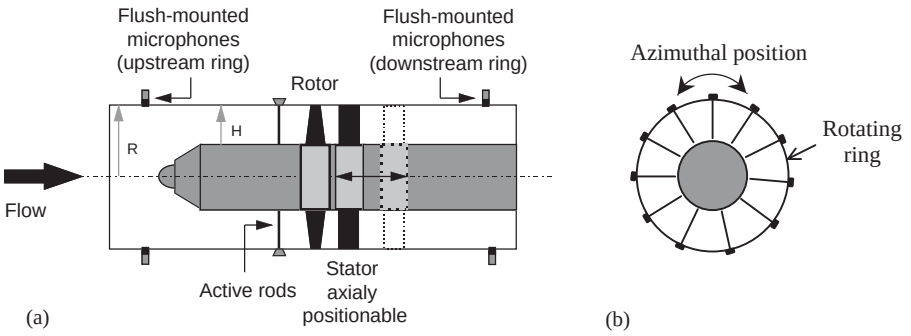

Fig. 2. Experimental set-up: (a) instrumented compressor model and (b) wake generator (rods).

4. Experimental results

In order to obtain the modal structure of the in-duct acoustic field due to rotor/stator interaction, a first series of runs is performed without the control grid. This mainly allows one to evaluate the intensity of the angular mode $m = -4$ on BPF, for several rotation speeds. This value will "have to be reached" when the grid is interacting with the rotor (stator off).

The frequency spectrum relative to a selected microphone of both upstream and downstream rings is presented in Fig. 3, for a rotation speed equal to 2500 r.p.m., and an axial mean Mach number of 0.13. The BPF tone ($f = 29$ N) is largely dominant compared to the second (58 N) and third (87 N) BPF harmonics, and about 40 dB above the broadband noise level (highly reduced by the averaged synchronous analysis used). Usual level differences between downstream and upstream measurements can be due to convected swirl effect and to rotor screen effect, not studied here. Anyway, the present investigations only concerns the upstream region.

The corresponding modal analyses relative to the BPF are shown in Fig. 4. The interaction mode measured by the upstream and downstream rings is clearly dominant. A sound pressure level (SPL) around 117 dB on the interaction mode $m = -4$ is measured upstream.

In order to evaluate the grid/rotor interaction mode, the next step consists of performing the same measurements with rods mounted and stator off. The modal spectrum for this case is shown in Fig. 5. The level of the upstream mode $m = -4$ is found to be clearly dominant (124 dB), but 7 dB higher than the rotor/stator interaction mode of Fig. 4 (117 dB). This is satisfactory as a first result, considering the rough approach used for the design. Nevertheless, the rod diameter appears to be slightly too large. Unfortunately, by decreasing the rod diameter, adequate rigidity of the system could not be ensured anymore. Hence, the reduction of the mode level is achieved by decreasing the length of the rods (cutting the end close to the hub). Since a simple relation between the rod length and the interaction mode level was not obvious at this stage of the study, the suitable value was found experimentally. Thus, using cut rods of 32 mm in length from the casing leads to the mode spectrum of Fig. 6. The spinning mode levels relative to both interaction configurations are plotted in this figure. Grid/rotor and rotor/stator interaction mode intensities are now very close (0.2 dB discrepancy). Moreover, the levels of the other modes are roughly balanced in the same way.

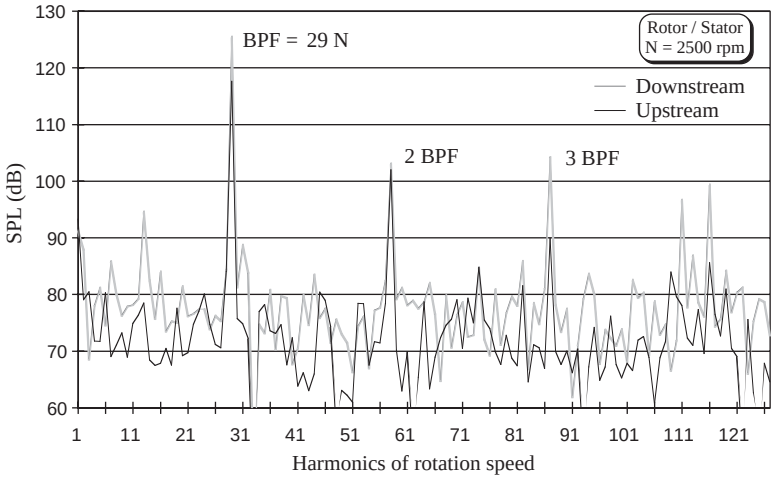

Fig. 3. Rotor–stator frequency spectrum.

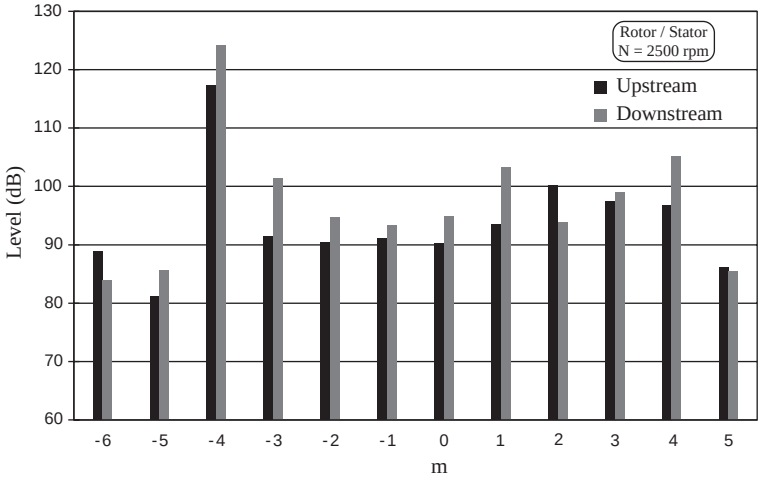

Fig. 4. Rotor–stator angular wave number spectrum at the BPF.

Following this result, the complete configuration grid–rotor–stator can be tested using a manual phase control. The interaction mode level with ANC-like system is plotted versus rod azimuthal position in Fig. 7a. They are compared to the rotor/stator interaction mode level previously found without noise control. The acoustic benefit provided by the system is high, with a reduction of about 8 dB corresponding to an azimuthal rod position for which grid/rotor and rotor/stator interaction modes are out of phase. The frequency spectra obtained with and without noise control are presented in Fig. 7b. They enable one to evaluate the performance of the system with respect to the overall tone level. A level reduction of 8 dB is found at the BPF, but the noise control increases the tones at 2 and 3 BPF by 8 and 15 dB, respectively. Nevertheless, these tones remain clearly below the BPF, and the ANC-like system provides an overall tone noise reduction of about 6 dB.

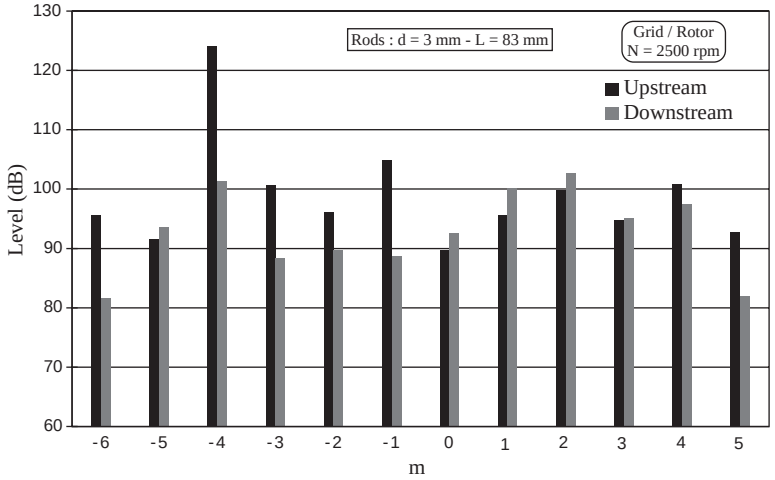

Fig. 5. Grid–rotor angular wave number spectrum at the BPF.

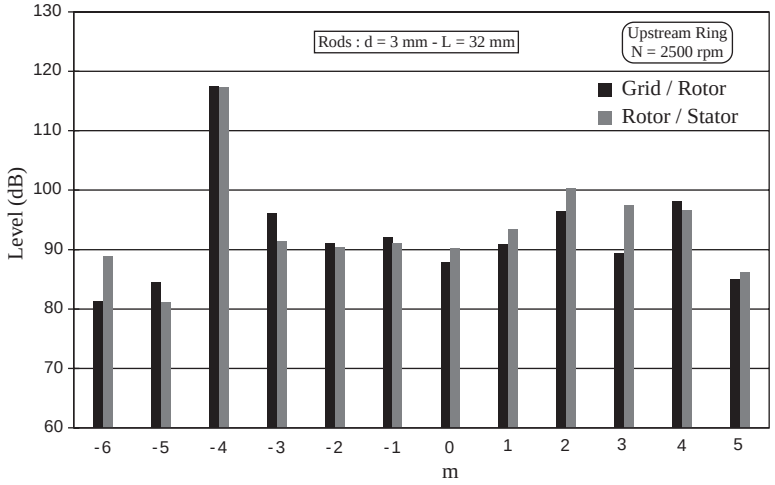

Fig. 6. Rotor–stator and grid–rotor wave number spectrum comparisons at the BPF.

5. CFD computations

For CPU costs reasons, CFD was performed using the COLIBRI code, which is a 2.5 D version of CANARI ONERA code. The unsteady averaged Navier–Stokes compressible equations solved by COLIBRI are detailed in Ref. [14]. The code is built on a multi-domain approach using structured grids. A four-step Runge–Kutta scheme for time integration is associated with a cell–vertex approach using a finite volume technique for space integration. Implicit residual smoothing allows the use of high values of the CFL number with a constant time step. Turbulence effects are included here by the use of the algebraic mixing length model of Michel. Boundary conditions, for

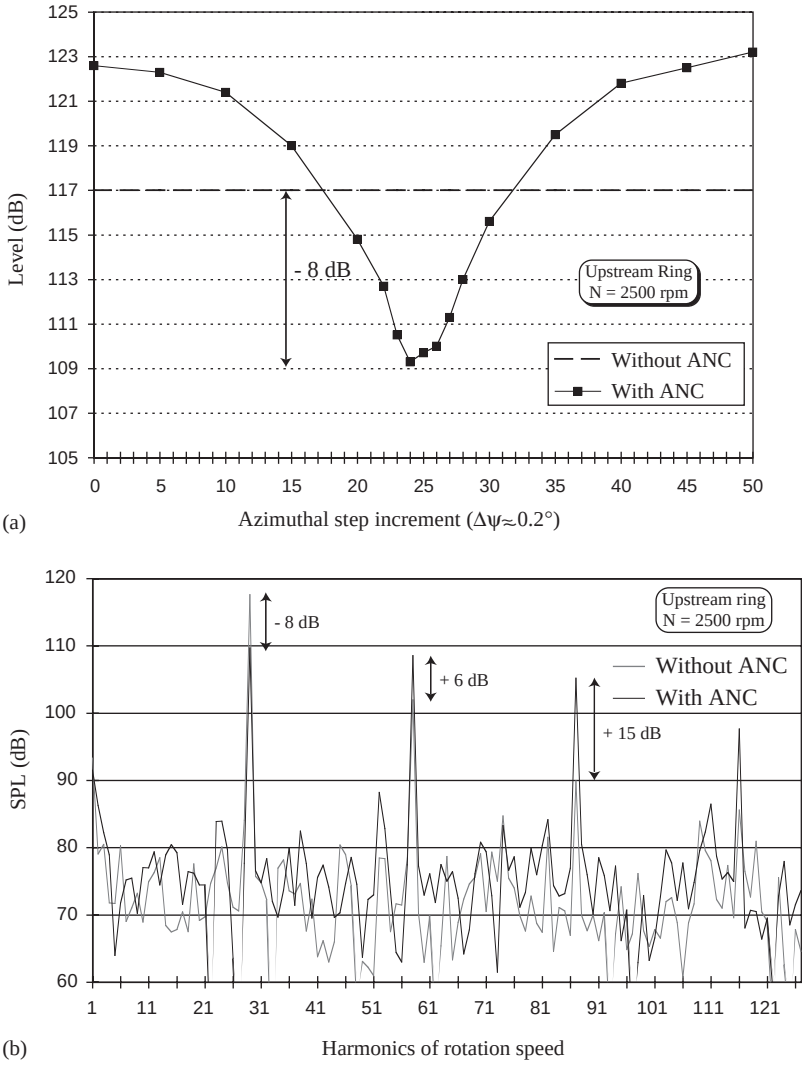

Fig. 7. Noise reduction obtained using the noise control system: (a) interaction mode level ($m = -4$) and (b) tone noise level.

inlet injection, outlet ejection, continuity boundaries and periodical boundaries, are related to characteristic-based relations. The reduced blade count (RBC) technique [24] allows the reduction of the number of computed blade-to-blade sections. Widely tested for several years at ONERA, this method takes into account the real geometry (without modification of the pitch) and the real rotor rotation speed. This technique is based on the idea that the blade to vane number ratio B/V can be approached by a ratio B_r/V_r where B_r and V_r are blade and vane numbers lower, respectively, than B and V.

Two configurations are studied: (1) The rotor–stator case, which gives the reference levels without using noise control (Fig. 4). (2) The rods–rotor case, which provided the optimal

balancing levels during the tests (Fig. 6). Computations are run at spanwise ratio $r/R = 0.92$, in order to compare CFD results with aerodynamic measurements available for this station.

5.1. Rotor–stator case

The mesh is constructed to fit the requirement of a high-density grid for a correct capture of viscous phenomena. In addition, regularity in the cells size evolution near the boundary between two wheels is investigated to improve the unsteady computations. There is an O mesh wrapping around each airfoil, and a special H grid topology to smoothly connect the blade passages of the rotor and the stator.

Using RBC, the B/V ratio is simplified from $\frac{29}{33} \approx 0.879$ to $\frac{7}{8} = 0.875$, so that it remains roughly constant. The CFD mesh is plotted in Fig. 8, showing only one point over two in each direction. The complete mesh size is about 137 000 nodes for seven rotor passages and eight stator passages. In the tangential and axial directions, the cell dimension is nearly 1 mm except in boundary layers. Normal to the blade surface, the cell size is 5 μm at the wall.

In order to visualize the convection of the rotor wake, instantaneous entropy iso-contours are shown in Fig. 9. The interaction between blade wakes and the stator vanes is clearly seen. To check the reliability of aerodynamic outputs, the steady forces on blade and vane, split into axial (thrust) and tangential (drag) components, are compared to experiment. Steady forces have been computed by time averaging the axial and tangential components of the momentum. They are compared to measurements in Table 2. A rather good agreement is found, since discrepancies are within 5%, except for the computed stator axial force, which is 9% higher than experiment.

Unsteady force components on blade and vane are then Fourier transformed, as required for acoustics (see next section). Results are summarized in Fig. 10. Unsteady thrust on the rotor, due to the potential flow interaction, is found to be higher than on the stator (due to wake interaction). This unexpected result shows that acoustic sources have to be considered both on blade and vane for the acoustic computations. Note that only first order loading harmonic on rotor ($j = 1$ in Eq. (1) and in Fig. 10a) and on stator ($n = 1$ in Eq. (1) and in Fig. 10b) are required for acoustics to compute the interaction mode $m = -4$.

5.2. Rods–rotor case

The V'/B ratio is simplified from $\frac{11}{29} \approx 0.379$ to $\frac{7}{8} = 0.375$ using the RBC approach. The CFD mesh is shown in Fig. 11 (also plotted one point over two in each direction). The same topology is

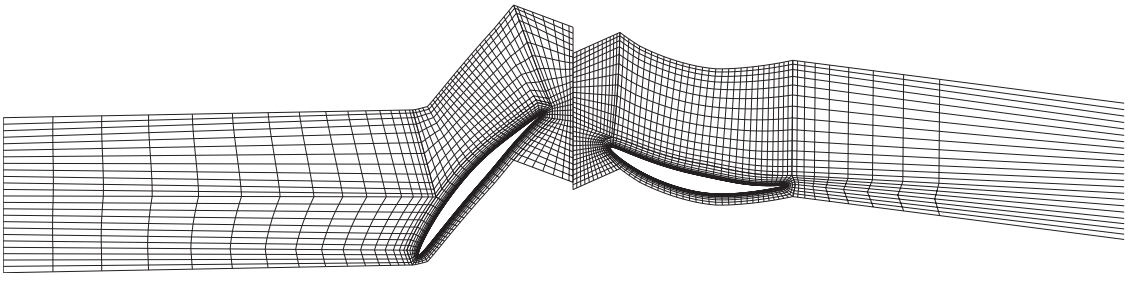

Fig. 8. COLIBRI mesh used for rotor–stator case.

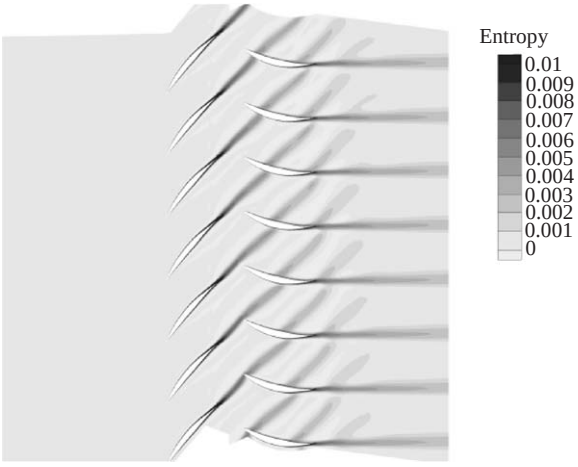

Fig. 9. Instantaneous entropy for rotor–stator case.

Table 2
Computed and measured steady force densities

	Rotor		Stator	
	Axial ($N\,m^{-1}$)	Tangential ($N\,m^{-1}$)	Axial ($N\,m^{-1}$)	Tangential ($N\,m^{-1}$)
CFD	54.2	−44.8	7.96	40.4
Experiment	55.9	−46.9	7.27	41.4

used. The complete mesh size is about 107 000 nodes for three rod-to-rod passages and eight rotor blade passages.

As for the previous case, entropy is shown in Fig. 12. Karman vortex streets behind the rods are clearly visible, which could make the use of an algebraic turbulence model (as Michel model used here) almost doubtful in such a case. Furthermore, since each vortex emission is not in phase, periodicity should not be accurately achieved in the three rod-to-rod passages, which does not verify the periodical boundary condition required when applying the RBC technique. Nevertheless, unsteady aerodynamics provided with the RBC approach is assumed to be usable for acoustics.

In order to verify that the aerodynamic penalties due to the rods are low, steady blade force components can be compared to those given in Table 2. As expected, the tangential component is unchanged (difference lower that 2‰), and discrepancy relative to the axial component is found to be lower than 4‰. This emphasizes the potential of such device regarding with applications.

In spite of the presence of Karman vortex streets, unsteady load spectra of Fig. 13 show that the loading harmonics on the rotor blade are found to be highly dominant compared to the other components (not shown) due to non-periodicity. Loads on the rods are of course negligible. Moreover, the third loading harmonic ($j = 3$ in Eq. (1)), which is at the origin of interaction mode $m = -4$, has the same order of magnitude as first loading harmonic in Fig. 10a. This seems to be well suited to the acoustic models presented in the next section.

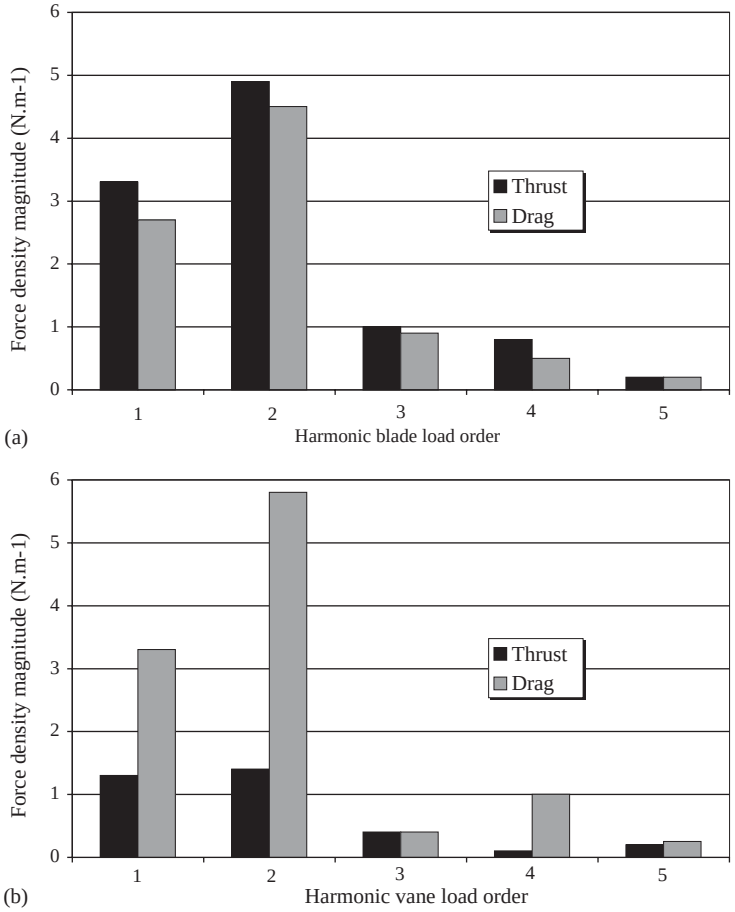

Fig. 10. Unsteady force density components for rotor–stator case: (a) rotor and (b) stator.

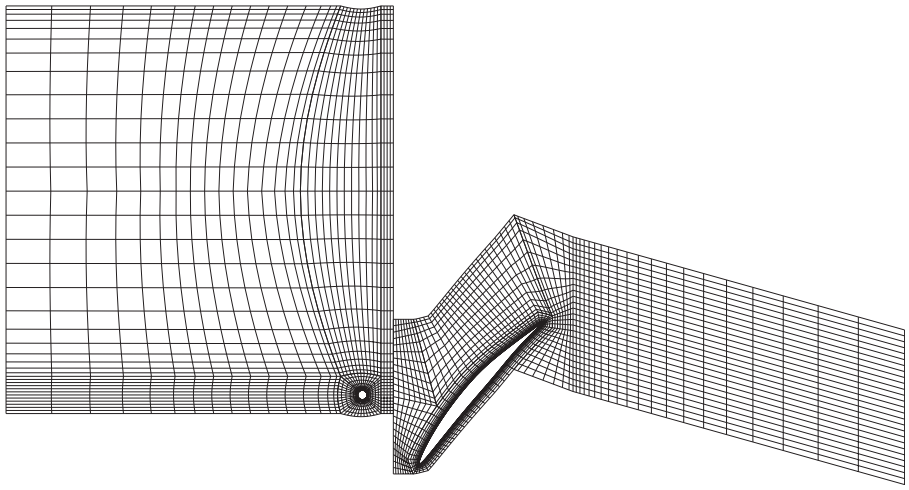

Fig. 11. COLIBRI mesh used for rods–rotor case.

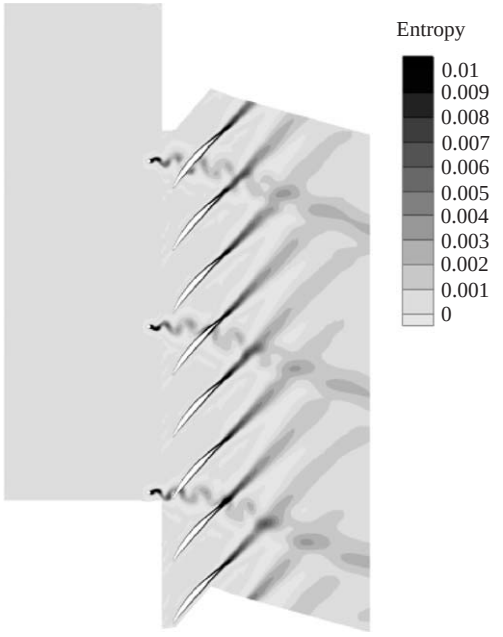

Fig. 12. Instantaneous entropy for rods–rotor case.

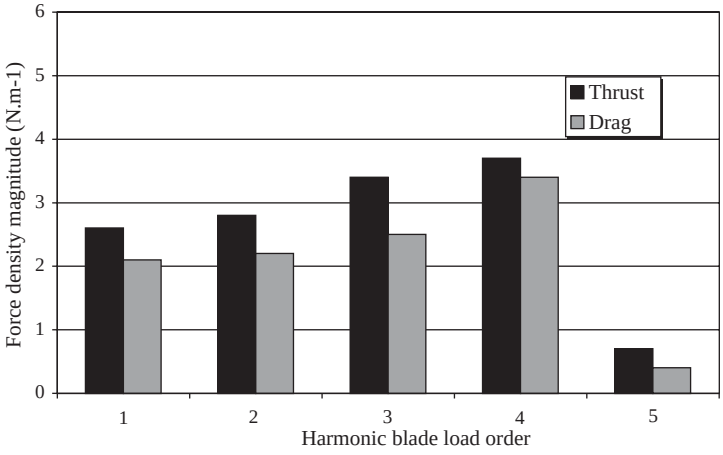

Fig. 13. Unsteady blade force density components for rods–rotor case.

6. Acoustic computations

The present acoustic model uses aerodynamic blade loads as inputs. It should be more reliable than a CFD-CAA matching-based approach, also described in Ref. [12] and used in Refs. [25–27], since the pressure disturbances taken upstream of the fan, as required for the matching, are not generally found to be accurate enough. Furthermore, 2-D input data, as those provided by COLIBRI, can be directly used here (whereas the matching would require 3-D CFD).

Interaction noise is expressed by the loading noise term of the FW–H equation. It can be written in the frequency domain as

$$p(\omega, M) = \int_S \int_\tau l_i \frac{\partial G}{\partial y_i} \mathrm{d}S \, \mathrm{d}\tau, \tag{2}$$

where l_i are the blade (or vane) unsteady loads along chordwise and spanwise directions. G is the Green function, solution of the Helmholtz equation in the presence of a Dirac point source $\delta(M–y_i)$. M is the observer (microphone) location, and y_i are the source co-ordinates in the fixed frame linked to the stator.

In the case of an infinite annular duct, G can be analytically calculated from first and second kind Bessel functions, and Eq. (2) can be expanded into spinning modes (m, μ) as done in Refs. [12,28]. Assuming chord compactness, the loads are split into axial thrust, T, and azimuthal drag, D, the radial component being neglected as done in Ref. [16]. Unsteady components are Fourier transformed, and complex values are needed to preserve any information relative to phase. Forces are provided either in the rotating (rotor blade) or in the fixed (stator vane) frame, depending on source locations. This leads to the following formulations for a point source:

(a) *Source on rotor (B blades)*:

$$p_{m\mu}(\omega_n, M) = \mathrm{i}\frac{B}{N}\left(k_z \hat{T}_{jV} + \frac{m}{r_s}\hat{D}_{jV}\right) G_{m\mu}\delta(m \pm jV - nB), \tag{3a}$$

where $\omega_n = 2\pi nBN$, i is a complex number, jV is the harmonic order of blade force density ($\mathrm{N\,m^{-1}}$), k_z is the axial wave number which depends on m and μ, and r_s is the radial co-ordinate of the source. Superscript on T and D means Fourier series.

(b) *Source on stator (V vanes)*:

$$p_{m\mu}(\omega_n, M) = \mathrm{i}\frac{V}{N}\left(k_z \hat{T}_{nB} + \frac{m}{r_s}\hat{D}_{nB}\right) G_{m\mu}\delta(m \pm jV - nB), \tag{3b}$$

where nB is the harmonic order of vane force density ($\mathrm{N\,m^{-1}}$).

Eqs. (3a) and (3b) can be evaluated using the analytical Green function of an infinite annular duct. This will be referenced as the infinite duct theory solution when discussing the computation results. Note that because the BEM solver used is only valid for a fluid at rest (see below), mean axial Mach number is also set equal to zero when calculating G and k_z. The no-flow assumption is justified by the fact that the in-duct mean flow is very low ($M = 0.13$) and so that flow effects on acoustic propagation can be neglected.

In order to take into account in-duct propagation and reflection effects in the presence of the real inlet geometry, previous FW–H formulations are coupled to a BEM scattering code, in the same way as in Refs. [12,18]. The BEM module of the commercial code SysNoise solves the Helmholtz equation, which assumes the fluid to be at rest. Since the problem is axisymmetric, axi-BEM computations can be performed. They are easy to implement (axi-line mesh only is required) and are quite fast. The coupling is simply achieved by replacing G by G^* in the previous equations, where (*) superscript denotes the solution of the bounded-space problem computed with BEM. In general, this solution cannot be split anymore into radial modes (in particular when the observer is outside the duct). For this reason, G^* is only expanded in angular modes m. Moreover, although the axial-wave number should not be defined anymore, aiming to have the

same expressions, a "modified" wave number, k_z^*, can be identified to k_z in Eqs. (3a) and (3b) by writing

$$k_z^* = \frac{-\mathrm{i}}{G_m^*}\left(\frac{\partial G_m^*}{\partial z}\right)_{y_i}.$$

The computation of k_z^* requires the calculation of the axial derivative of G_m^*, which is made numerically using a centred finite difference from two adjacent source locations (y_i) along the cylinder axis direction.

Using COLIBRI, the loads are computed in terms of a force density (expressed in Newton per meter) at one selected spanwise station only. A radial scanning would require as many COLIBRI runs as stations desired. As a first step, an issue for this problem is to consider each loading harmonic to be equally distributed along the span. Although it can appear to be a gross approximation, this assumption may be justified by the fact that the hub-to-tip ratio is rather high ($h = 0.67$), and that the vanes are straight. In this way, acoustic sources are generated as a dipole line source. Moreover, because the acoustic wavelength to be studied is large compared to H, and because only the first radial mode is cut-on in the annular region, amplitude and phase of the Green function are almost constant with respect to radial position of the source (perpendicularly to the duct axis). This last point has been checked analytically, and numerically with BEM. Thanks to these simplifications, $\hat{T}$, $\hat{D}$, G^* (or G), and so k_z^* (or k_z), can be put outside from the integral, so that radial integration is analytically achieved. Thus, integrating Eqs. (3a) and (3b) along r leads to (only (*) formulations given):

$$p_m(\omega_n, M) = \mathrm{i}\frac{G_m^* B}{N}\left[k_z^* \hat{T}_{jV} R(1-h) + m\hat{D}_{jV}\ln\left(\frac{1}{h}\right)\right], \tag{4a}$$

$$p_m(\omega_n, M) = \mathrm{i}\frac{G_m^* V}{N}\left[k_z^* \hat{T}_{nB} R(1-h) + m\hat{D}_{nB}\ln\left(\frac{1}{h}\right)\right]. \tag{4b}$$

A 3-D representation of the mesh used for BEM computations is shown in Fig. 14. To compute G_m^*, a source point, with angular frequency ω_n and angular wave number m, is placed at mid-height and at a suitable axial position, corresponding to the compacted-force point provided by COLIBRI. In-duct propagation results are shown in Fig. 15, on which the microphone position used to compute the Green function is also indicated. Note that because focus is only on upstream propagation, a non-reflecting boundary condition is used at the outlet section to ensure the outgoing acoustic waves to be fully transmitted downstream. Standing waves are found upstream, due to the transition from annular to cylindrical sections, showing the importance of scattering effects and the requirement for coupling with BEM.

7. Comparison of experimental and numerical acoustic results

Acoustic calculations based on the above equations have been performed using the unsteady loads provided by COLIBRI. The rotor–stator interaction mode level is achieved by the coherent sum of the contributions of both potential flow interaction (Eq. (4a)) and wake interaction (Eq. (4b)). The rods–rotor configuration is computed in two steps. Firstly, full-length rods

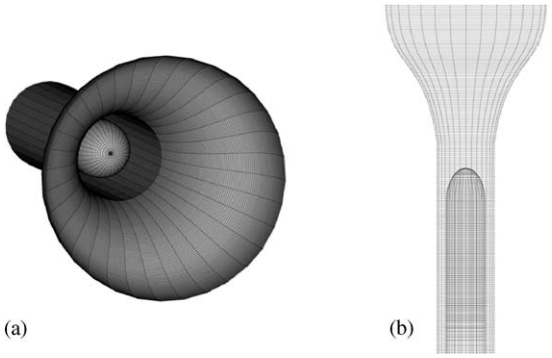

Fig. 14. BEM grid (3D representation): (a) front view and (b) top view.

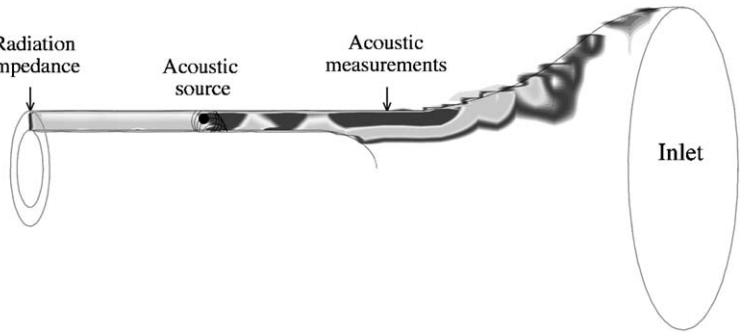

Fig. 15. Green's function computation using BEM.

($L = 83$ mm) are considered to compare with results of Fig. 5. COLIBRI post-processed outputs are directly applied to Eq. (4a). Secondly, a simulation is performed to relate to the optimal configuration with shorter rods ($L = 32$ mm). This is simply achieved by fitting the range of radial integration ($H = 83$ mm) to the length of the rods ($H = 32$ mm), that is to say by increasing h ($h = 1 - H/R$) from $h = 0.67$ to $h = 0.87$ in Eq. (4a).

Interaction mode levels in each configuration are summarized in Table 3, where the infinite duct theory solution is also given. By comparison to the infinite duct theory, coupling with BEM provides much better predictions that are within 1.5 dB of the measurements. These are very promising results, since more accuracy cannot be expected from 2-D CFD and simplified source analogies for acoustics. In fact, it clearly confirms that for this considered case, geometrical effects (taken into account when coupling with BEM) are more important than the flow effects (neglected by the fluid at rest assumption) on acoustic propagation. Computed wakes behind rods as well as assumptions made on unsteady loads seem quite reliable regarding the accuracy of the predictions. Nevertheless, present computations are limited to a basic case at a single rotation speed, so that validations would have to be extended. Anyway, the optimal configuration experimentally achieved is verified by the numerical results, with only 1 dB discrepancy between rotor/stator and rods/rotor (cut rods) interaction mode predicted level.

Finally, the noise control system is simulated by linearly varying the phase of the rods–rotor contribution (as done during the tests) when adding, still in a coherent way, all contributions

Table 3
Comparisons between acoustic predictions and experiment at the BPF

Configuration	COLIBRI + FW–H/infinite duct (dB)	COLIBRI + FW–H/BEM (dB)	Experiment (dB)
Rotor/stator	116.1	117.2	117.3
Rods/rotor ($h = 0.67$)	119.9	122.8	124.3
Rods/rotor ($h = 0.87$)	113.2	116.3	117.5

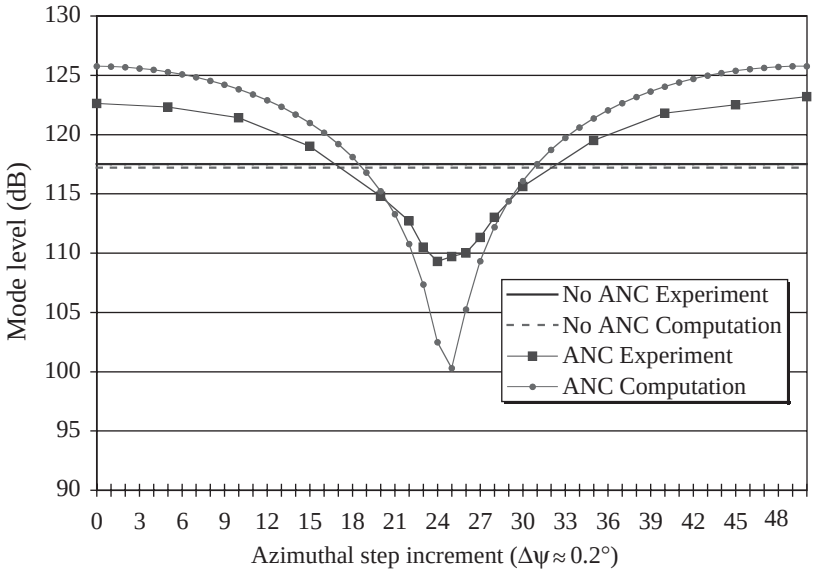

Fig. 16. Interaction mode reduction using the noise control system.

relative to the complete rods/rotor/stator configuration. The reduction of the interaction mode obtained in the tests using noise control is compared to the numerical solution in Fig. 16. The reference level without noise control is also indicated. The agreement between the two sets of results is quite satisfactory both in shape and level. Although the predicted levels for rotor–stator and rods–rotor ($h = 0.87$) interaction mode are not as close as in the tests, a very high reduction of SPL is obtained. Note that the level of discrepancy observed in Fig. 16 at maximum noise level reduction (−8 dB for measurements, −17 dB for computations), should probably be lower if a more refined step range were used during the tests (experimental curve is slightly flatter), and especially if the background noise were included in the computations.

8. Conclusions

An original noise control technique has been successfully applied to reduce rotor–stator interaction noise of subsonic fans. The wake generator system, made of a simple grid of cylindrical rods mounted upstream of the rotor, has been tested on the CERF compressor model. The

interaction of the control grid with the rotor generates a mode of the same order as the rotor–stator interaction mode, and of similar magnitude. Mounted on a rotating ring, the rods can be positioned in azimuth in order to adjust the phase of the control mode so that the two interaction modes are out of phase. The system provides a tonal noise reduction of 8 dB on the blade passing frequency (BPF). Although the acoustic power is partly re-distributed to higher harmonics (on two and three BPF), because higher modes are cut on, an overall discrete frequency noise reduction of about 6 dB has been achieved. The present study focused on BPF tone reduction, but it could be used for the reduction of the two BPF tone by selecting a suitable higher interaction mode. This would lead to another control grid design.

In addition, the system has been investigated in a numerical way. A 2-D unsteady Reynolds averaged Navier–Stokes solver (COLIBRI ONERA code), providing the unsteady blade and vane forces required as inputs for acoustics, has been coupled to a BEM code (SysNoise), solving the Helmholtz equation. Interaction noise sources are expressed by the Ffowcs Williams and Hawkings equation. Using suitable assumptions, simple formulations, written in the frequency-wave number domain, have been proposed and applied with success to the CERF rig configuration. Interaction mode levels predicted by the computations are within 1.5 dB of experiment. For the optimal tested noise control configuration, the computed maximum noise reduction is higher than measurements, but the efficiency of the system is found to be quite comparable. It is a very good result considering the complexity of the problem, which confirms the suitability of the assumptions made and partly validates the numerical tools involved.

In view of industrial applications, the next step should be the automation of the phase adjustment, using a real-time modal analysis process to feedback a motorized rotating ring, setting the rod position in azimuth. Thus, one would get a true active noise control (ANC) system. Another investigation could consist of applying the method to simultaneously reduce several interaction modes (by using multiple grids), in order to better decrease the levels of first and second harmonics.

In summary, contrary to other current ANC investigations, the system proposed here seems easier to implement, and should probably cause less penalties on aerodynamic performance, as shown by the steady force analysis.

Acknowledgements

This work has been supported by the X-Noise European projects RESOUND and TurboNoiseCFD. The authors would like to acknowledge S. Léwy and P. Malbéqui (ONERA, Numerical Simulations and Aeroacoustics Department) for their advice respectively on control grid design and in BEM.

References

[1] C. Polacsek, Reduction of fan rotor–stator interacting modes using a novel design: an experimental study, Proceedings of the Sixth International Congress on Sound and Vibration (ISCV), Copenhagen, 1999.

[2] J.M. Tyler, T.G. Sofrin, Axial flow compressor noise studies, SAE Transactions 70 (1962) 309–332.

[3] R.E. Kraft, K.B. Kontos, Theoretical implications of active noise control for turbofan engines, 15th Aeroacoustics Conference, Long Beach, CA, October 1993.
[4] R.H. Thomas, R.A. Burdisso, R.A. Fuller, C.R. O'Brien, Active control of fan noise from a turbofan engine, American Institute of Aeronautics and Astronautics Journal 32 (1) (1994) 23–30.
[5] T. Ishii, H. Kobayashi, H. Oinuma, Wave-form technique for reduction of tones radiated from a ducted fan, AIAA No. 97-1664-CP, 1997, pp. 619–625.
[6] S. Sawyer, S. Fleeter, Active control of discrete-frequency noise generated by rotor–stator interactions, AIAA No. 97-1663-CP, 1997, pp. 609–617.
[7] D.L. Sutliff, Z. Hu, F.G. Pla, L.J. Heidelberg, Active noise control of low speed fan rotor–stator modes, Third AIAA/CEAS Aeroacoustic Conference, Atlanta, GA, 1997.
[8] A.R.D. Curtis, Active Control of Fan Noise by Vane Actuators, BBN Technologies, Cambridge, MA, NASA/CR-1999-209156, 1999.
[9] W. Just, I.U. Borchers, H. Antoine, E. Bouty, J. Zillmann, R. Maier, Control of fan noise by active stators, Seventh AIAA/CEAS, Maastricht, 2001.
[10] P.A. Nelson, Active techniques, their potential for application in aeroacoustics, Sixth AIAA/CEAS, Lahaina, HI, 2000.
[11] S. Kamiyoshi, S. Kaji, Tone noise reduction of multi-stage fan by airfoil clocking, Sixth AIAA/CEAS, Lahaina, HI, 2000.
[12] C. Polacsek, Interaction noise computations in axisymmetrical turbofan inlets, Eighth International Congress on Sound and Vibration (ICSV), Hong Kong, China, 2001.
[13] V. Couaillier, Numerical simulation of separated turbulent flows based on the solution of a RANS/low Reynolds two-equations model, 37th AIAA/ASME, Reno, USA, 1999.
[14] I. Le Madec, Modélisation des Écoulements Transitionnels et Turbulents dans les Grilles d'Aubes de Turbomachines Suivant l'Orientation Turbines, Ph.D. Thesis, Rennes University, 1993.
[15] J.E. Ffowcs Williams, D.L. Hawkings, Sound generation by turbulence and surfaces in arbitrary motion, Philosophical Transactions of the Royal Society of London 264 (A1151) (1969).
[16] M.E. Goldstein, Aeroacoustics, McGraw Hill, New York, 1976.
[17] P. Malbéqui, C. Peyret, Fan noise radiation from the inlets of the future supersonic aircraft, Euronoise'98, Munich, 1998.
[18] E. Manoha, G. Elias, B. Troff, P. Sagaut, Towards the use of boundary element method in computational aeroacoustics, AIAA paper 99-1980, Fifth AIAA/CEAS Conference, Bellevue, WA, 1999.
[19] G. Fournier, J. Huard, J. Pérucchini, Noise reduction of fans by control of flow distorsion, Internoise, Yokohama, 1994, pp. 519–522.
[20] G.N. Abramovich, The theory of turbulent jets, Massachusetts Institute of Technology, 1963.
[21] L.D. Landau, E.M. Lifshitz, Course of Theoretical Physics, Institute of Physical Problems, 2nd Edition, Vol. 6, USSR Academy of Sciences, Moscow, 1987.
[22] N.H. Kemp, W.R. Sears, The unsteady forces due to viscous wakes in turbomachines, Journal of the Aeronautical Sciences 22(7) (1955).
[23] S. Kaji, T. Okazaki, Generation of sound by rotor–stator interaction, Journal of Sound and Vibration 13 (3) (1970) 281–307.
[24] A. Fourmaux, L. Dubois, Unsteady flow computation in double-stage double-shaft turbine, 14th ISABE, Florence, Italy, September, 1999.
[25] M.H. Dunn, J. Tweed, F. Farassat, The prediction of ducted fan engine noise via a boundary integral equation method, American Institute of Aeronautics and Astronautics Paper (1996) 96–1770.
[26] C.L. Rumsey, R.T. Biedron, F. Farassat, P.L. Spence, ducted-fan engine acoustic predictions using a Navier–Stokes code, Journal of Sound and Vibration 213 (4) (1998) 643–664.
[27] R.T. Biedron, C. Rumsey, G.G. Podboy, M.H. Dunn, Predicting the rotor–stator interaction acoustics of a ducted fan engine, 39th AIAA ASME, Reno, NV, 2001.
[28] S.W. Rienstra, Acoustic radiation from a semi-infinite annular duct in uniform subsonic mean flow, Journal of Sound and Vibration 94 (2) (1984) 267–288.